ELSEVIER

Coastal Engineering 32 (1997) 289–319

COASTAL ENGINEERING

Surf zone dynamics simulated by a Boussinesq type model. Part II: surf beat and swash oscillations for wave groups and irregular waves

P.A. Madsen *, O.R. Sørensen, H.A. Schäffer

International Research Centre for Computational Hydrodynamics (ICCH), Danish Hydraulic Institute, Agern Alle 5, 2970 Hørsholm, Denmark

Received 2 April 1997; revised 23 September 1997; accepted 23 September 1997

Abstract

This is the second of three papers on the modelling of various types of surf zone phenomena. In the first paper the general model was described and it was applied to study cross-shore motion of regular waves in the surf zone. In this paper, part II, we consider the cross-shore motion of wave groups and irregular waves with emphasis on shoaling, breaking and runup as well as the generation of surf beats. These phenomena are investigated numerically by using a time-domain Boussinesq type model, which resolves the primary wave motion as well as the long waves. As compared with the classical Boussinesq equations, the equations adopted here allow for improved linear dispersion characteristics and wave breaking is modelled by using a roller concept for spilling breakers. The swash zone is included by incorporating a moving shoreline boundary condition and radiation of short and long period waves from the offshore boundary is allowed by the use of absorbing sponge layers. Mutual interaction between short waves and long waves is inherent in the model. This allows, for example, for a general exchange of energy between triads rather than a simple one-way forcing of bound waves and for a substantial modification of bore celerities in the swash zone due to the presence of long waves. The model study is based mainly on incident bichromatic wave groups considering a range of mean frequencies, group frequencies, modulation rates, sea bed slopes and surf similarity parameters. Additionally, two cases of incident irregular waves are studied. The model results presented include transformation of surface elevations during shoaling, breaking and runup and the resulting shoreline oscillations. The low frequency motion induced by the primary-wave groups is determined at the shoreline and outside the surf zone by low-pass filtering and subsequent division into incident bound and free components and reflected free components. The model results are compared with laboratory

* Corresponding author. Fax: +45-45-762567; e-mail: icch@dhi.dk.

PII S0378-3839(97)00029-X

experiments from the literature and the agreement is generally found to be very good. Finally the paper includes special details from the breaker model: time and space trajectories of surface rollers revealing the breakpoint oscillation and the speed of bores; envelopes of low-pass filtered radiation stress and surface elevation; sensitivity of surf beat to group frequency, modulation rate and bottom slope is investigated. Part III of this work (Sørensen et al., 1998) presents nearshore circulations induced by the breaking of unidirectional and multi-directional waves.

Keywords: Boussineq model; Wave breaking; Surf zone; Surf beat; Irregular waves; Runup

1. Introduction

Shoaling, breaking and runup of irregular wave trains in shallow water is a nonlinear process involving a number of complicated details. Triad interactions between harmonics in shallow water lead to substantial cross spectral energy transfer in relatively short distances, and during shoaling still more energy will be transferred into bound sub-harmonics and super-harmonics, which travel phase locked to the primary wave train.

In a number of situations, however, part of the energy may be released as free harmonics, e.g. during the passage over submerged bars or during the process of breaking. When wave breaking occurs, the primary waves and their super-harmonics will start dissipating and this will allow for a gradual release of the bound sub-harmonics and result in free long waves moving towards the shoreline from which they will be almost fully reflected.

To some extent bound long waves will persist in the surf zone depending on the degree of groupiness in this region. The groupiness of the incident waves will generally be reduced by the breaking process, since high waves tend to break further offshore than low waves. However, some groupiness may persist and penetrate further into the surf zone. The groupiness may even be reversed during the transformation that takes place while the group undergoes the initial stages of breaking. This happens if the higher waves in a wave group decay sufficiently during breaking to appear as the lower waves further inshore. The individual waves in a group will break at different depths, which will result in a horizontal variation of the breakpoint. The excursion of the breakpoint will depend on the groupiness of the incident waves, and while a linear sinusoidal motion can be expected for a weakly modulated bichromatic group, this is modified for a fully modulated group where the shoreward extreme of the breakpoint will in principle be at the shoreline. The motion of the breakpoint will result in large time-varying radiation stress gradients in the region of incipient breaking and this will act as a local forcing of free long waves at the group frequency and its higher harmonics. These free waves will propagate in the onshore and offshore directions. Since the breakpoint-forced long waves are basically due to variations of the starting point for the setup, the phenomenon is sometimes referred to as dynamic setup.

The incident bound long waves will coexist with the breakpoint-forced long waves emitted in the shoreward direction and after the reflection at the shoreline they will again take part in the interference pattern with the breakpoint-forced waves being emitted directly seawards. Hence the relative phases of the different wave systems will be important for the resulting free long waves radiating in the offshore direction.

Publications by Tucker (1950), Longuet-Higgins and Stewart (1962), Symonds et al. (1982), Freilich and Guza (1984), Schäffer (1993) and others have significantly improved the understanding of the above processes. The relative importance of the bound and breakpoint-forced long waves is, however, yet an open question. In laboratory experiments with bichromatic waves (on a slope of 1/20) Kostense (1984) found that the amplitudes of the outgoing free long waves depend on the group frequency in a non-monotonic fashion, indicating a significant influence from the moving breakpoint mechanism. On the other hand such a frequency dependence was absent in the field observations (on a slope of 1/40) analyzed by List (1992), which may partly be due to the multi-directionality and irregularity of the wave field which tend to smear things out. List suggested that the moving breakpoint mechanism is important only in the case of steep seabed profiles, but this conclusion is not supported by the present work as discussed in Section 5.

Previous work on the modelling of nearshore low-frequency waves has mainly been based on the wave-averaged approach using linear theory for the primary waves and their radiation stresses combined with linear or nonlinear equations of motion for the long waves (e.g. Symonds et al., 1982; Lo, 1988; Schäffer, 1990; List, 1992; Roelvink et al., 1992). The use of wave-averaged models to predict low-frequency motion is obviously a very cost efficient way of studying the processes in the nearshore. The disadvantage of the wave-averaged approach is however, that it generally suffers from a number of questionable assumptions concerning the primary wave motion. In reality this wave motion is strongly nonlinear and will be fully coupled with the low-frequency motion e.g. in the swash zone where depth variations and velocity variations due to the long waves will influence the primary wave motion. An example of a fully coupled approach was given by Watson and Peregrine (1992) and Watson et al. (1994), who used the nonlinear shallow water equations to describe the combined short and long period motions in the inner surf zone.

The present paper concentrates on cross-shore motions of wave groups and on the verification of a time-domain Boussinesq type model extended to include the surf zone and the swash zone. The model resolves the primary waves as well as the low frequency motion and allows for a study of the nonlinear processes involved in shoaling, breaking and runup of irregular wave trains. A detailed description of the model was given in part I (Madsen et al., 1997), while a brief summary can be found in Section 2, which also includes discussions of previous analytical and numerical models of surf beat. Section 3 concerns the evolution of the surface elevation through the surf zone and the shoreline motion due to a range of incident bichromatic wave trains and two cases of incident random waves. The model results are verified against various laboratory experiments. Section 4 concerns the surf beat induced by a range of incident bichromatic wave trains with emphasis on the amplitude of the outgoing free long waves. The model results are verified against laboratory experiments of Kostense (1984). Finally, further investigations of surf beat are presented in Section 5, where we present details from the primary wave motion as well as from the low frequency waves: This includes e.g. roller trajectories, speed of bores, oscillation of breaker line and shoreline, envelopes of surface elevations and low-pass filtered elevations, envelopes of low-pass filtered radiation stress gradients, and the influence of group frequency, modulation rate and bottom slope on the surf beat.

2. Analytical and numerical models of surf beat

Munk (1949) and Tucker (1950) originally introduced the expressions 'beats of surf' or 'surf beats' to describe low frequency waves with periods of the order of minutes. Field measurements of these waves were found to be similar to the envelope of the swell except for a time lag of several minutes. Munk and Tucker suggested that the mass transport associated with high groups of swell would be reflected from the beach after wave breaking, leading to the observed substantial time lag. For a number of years, however, it remained a mystery why high groups of incoming swell were associated with a negative pressure pulse.

Longuet-Higgins and Stewart (1962) explained this phenomenon by their theory of radiation stress and bound long waves forced by wave groups. They suggested that while the short waves penetrate into shallow water, where they are destroyed due to wave breaking, the bound long waves may be partially reflected on the sloping beach. A model for this mechanism was, however, not given in detail.

Symonds et al. (1982) were the first to account for the conditions at the breakpoint and inside the surf zone in a theoretical model of surf beat. They discussed how the total setup at the shoreline depends on the width of the surf zone, and suggested that the time variation of the breakpoint position, introduced by incident wave groups of varying amplitude, will lead to the generation of free waves at the group frequency (and its harmonics). They considered the case of weakly modulated incident waves and derived an analytical forcing function corresponding to a sinusoidal variation of the breakpoint. Inside the surf zone the modulation or groupiness of the incident waves was assumed to vanish and the wave height was taken to be a fixed proportion of the local water depth. The low-frequency motion was described by the linearized shallow water equations driven by radiation stresses derived from linear wave theory. Incoming bound long waves and frictional effects were neglected.

Schäffer (1990, 1993) improved the theoretical model of Symonds et al. in a number of ways of which the inclusion of the incoming bound long waves and their transformation on a sloping beach turned out to be most important for the results. He also considered different types of surf zone models for the incident primary waves: The first one was the saturation approach by Symonds et al. (1982), neglecting groupiness inside the surf zone. The second one assumed a fixed breakpoint position but allowed for full transmission of groupiness into the surf zone. The model finally adopted was a hybrid between the two allowing the transmission of groupiness to be zero, partial, full or even to represent a reversion of groupiness. A comparison with the experiments by Kostense (1984) showed a significant improvement relative to the simpler model of Symonds et al. (1982), but the general trend was a clear overestimation of the surf beat.

List (1992) presented a numerical model of surf beat based on linear shallow water theory for the low frequency motion as well as for the primary waves. Like Schäffer

(1990, 1993) both bound and breakpoint-forced long waves were included in the description but as a new feature the radiation stress terms were allowed to have an arbitrary time variation. A wave by wave approach was used to propagate time series of wave heights combining Green's shoaling law with a saturation constraint of constant maximum wave height to water depth ratio. Unfortunately, it appears that the use of shallow water theory for the primary waves (i.e. neglecting dispersion) is a serious limiting factor for the applicability of List's surf beat model: Generally exact resonance in the long wave equations is modified to near resonance by dispersion in the primary waves and by the bottom slope term. For this reason the forcing of bound waves can be expected to be significantly overestimated in List's model.

Roelvink et al. (1992) and Roelvink (1993) presented a numerical surf beat model based on a nonlinear description of the low frequency motion and a linear description of the primary waves. The low frequency motion was determined by solving the nonlinear shallow water equations including time-varying radiation stress and bottom friction, while the primary wave motion was determined by solving an energy balance equation including dissipation terms due to wave breaking. As a special feature the surf beat model included part of the feed back from the low frequency motion to the primary wave motion, viz. the influence of the water level fluctuations on the group velocity and dissipation of energy. The formulation of wave breaking was inspired by the criterion of Battjes and Janssen (1978) for random waves, but modified to account for bichromatic wave groups as well. The case of irregular waves was treated by using the narrow-band approximation, implying that the energy propagates at a single group speed. Roelvink verified the model on the case of incident bichromatic waves as well as on irregular waves. In the former case a fairly good agreement with the bichromatic experiments by Kostense (1984) was obtained for a particular calibration of model parameters. In the latter case a comparison with the random wave experiments by Van Leeuwen (1992) left something to be desired, and the computed short wave energy near the shoreline was significantly underpredicted and out of phase, while the low frequency motion was qualitatively acceptable. The discrepancies obtained in the case of irregular waves was most likely caused by Roelvink's narrow-band approximation, which assumes short-wave energy to propagate with constant form, while in reality wave groups are gradually transformed even on a horizontal bottom.

Watson and Peregrine (1992) presented a fully coupled description of the wave dynamics in the swash zone by using the nonlinear shallow water (NSW) equations to resolve the primary wave motion as well as the long waves. A shock-capturing method allowed for an automatic treatment of bores without the need for any special tracking algorithm and the moving shoreline due to the combined low-frequency and primary wave motion was represented in a fixed grid system. Compared to the wave averaged models the approach by Watson and Peregrine has the advantage that it includes the substantial shoreline excursion due to the total wave motion and the modification of the propagation speed of the incident primary waves due to the presence of the long waves. The major limitation of the method is, however, the lack of frequency dispersion, which has undesirable implications on both bound wave generation and breakpoint position and restricts applications to the inner surf and swash zone.

The numerical model used in the present work is based on two-dimensional Boussinesq type equations formulated in the time-domain, and it features improved linear dispersion characteristics, possibility for wave breaking, and a moving boundary at the shoreline. The model is described in detail in part I (Madsen et al., 1997) and is briefly summarized in the following: The model of wave breaking is based on the concept of surface rollers and applies to regular as well as irregular waves. Breaking is predicted to occur when the local slope of the surface elevation exceeds an initial critical value, $\tan \phi_B$, using $\phi_B = 20°$. During the transition from initial breaking to a bore-like stage in the inner surf zone, the critical angle is assumed to gradually change from ϕ_B to a smaller terminal angle, ϕ_0 which is taken to be 10°. The roller thickness is determined geometrically as the water above the tangent of slope $\tan \phi$ and the resulting thickness is multiplied by a shape factor. The influence of breaking on the governing equations is modelled by an additional convective momentum term originating from a non-uniform velocity profile induced by the roller. The local phase celerity is an important part of this formulation and it is determined interactively. Bottom friction is described by the classical quadratic friction law with a friction coefficient f_w of 0.01. Finally a moving shoreline is incorporated in the model by replacing the solid beach by a permeable beach characterized by an extremely small porosity. This allows for the determination of wave motion in the swash zone and it provides a shoreline condition which like a natural beach tends to be reflective for waves of small steepness viz. the low frequency waves.

3. Evolution of surface elevations and shoreline motion

In this chapter the numerical model is verified on breaking and runup of irregular wave trains with emphasis on the evolution of surface elevations as well as the shoreline motion. A few spectral measures will also be given such as the significant wave height, the skewness and the asymmetry. The first part of the section concerns the case of incident bichromatic wave groups, while the second part concerns incident irregular wave trains.

3.1. Bichromatic wave groups on a sloping beach

In recent publications Mase (1994, 1995) presented experimental results for shoaling, breaking and runup of various types of bichromatic wave trains on a gentle slope. Fig. 1 illustrates the experimental setup. The flume consists of a 10 m horizontal section with a

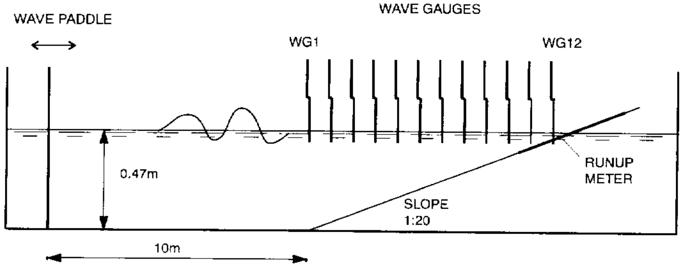

Fig. 1. Sketch of physical wave flume (Mase, 1994).

water depth of 0.47 m and a 12 m section with a constant impermeable 1/20 slope. Twelve wave gauges of capacitance type are installed at still water depths of 47, 35, 30, 25, 20, 17.5, 15, 12.5, 10, 7.5, 5 and 2.5 cm, and they are denoted WG1 to WG12. Furthermore, a runup meter is placed at the shoreline. Mase considered three different patterns of bichromatic waves of which we shall concentrate on the two, which can be described by the following equation

$$\eta = a_1 \cos(2\pi f_1 t) + a_2 \cos(2\pi f_2 t) \tag{3.1}$$

where

$$f_1 = \left(1 + \frac{\Delta}{2}\right) f_m, \qquad f_2 = \left(1 - \frac{\Delta}{2}\right) f_m \tag{3.2}$$

By choosing a_1 equal to a_2 and Δ equal to 0.2 and 0.1, Mase described two different types of fully modulated wave groups, WP1 and WP2 consisting of five and ten individual waves respectively. For each type the mean frequency, f_m was taken as 0.3, 0.4, 0.5, 0.6, 0.8, 1.0 and 1.2 Hz. Additionally, three different energy levels were considered for each frequency and wave pattern. In the following we shall concentrate on the case of medium energy level.

The variation in mean frequency from 1.2 to 0.3 Hz represents a significant change in wave conditions, which are listed in Table 1 in terms of h/L_0, H_0/L_0 and ζ_0, where L_0 is the deep water wave length based on the mean frequency, H_0 is an estimate of the maximum wave height in the wave group (at deep water) and h is the water depth taken at the toe of the slope. The surf similarity parameter (ζ) is defined as usual as the beach slope divided by the square root of the deep water wave steepness and we denote it ζ_0 when based on H_0/L_0, the steepest wave in the group. Based on the classification of Galvin (1968) of wave breaking, Battjes (1974) found that spilling breakers would occur for $\zeta < 0.5$, while plunging would occur for $0.5 < \zeta < 3.3$. Within a wave group the highest waves may be spilling while the lowest ones are plunging. Looking at the wave height distribution we may identify the probability of plungers versus spillers by separating the two categories at the wave height corresponding to $\zeta = 0.5$ (last column in Table 1). Even for the highest mean frequency, where spilling breakers prevail, plunging is expected for the waves near the node of the group. All waves are plunging at the lowest mean frequency. A few percent surging breakers ($\zeta > 3.3$) occurring for $f_m = 0.3$ Hz are counted as plungers.

Table 1
Wave characteristics of test cases by Mase (1994)

Mean frequency (Hz)	h/L_0	H_0/L_0	ζ_0	Plungers:Spillers (percentages)
1.2	0.43	0.092	0.16	7:93
1.0	0.30	0.064	0.19	9:81
0.8	0.19	0.041	0.24	14:86
0.6	0.11	0.023	0.32	26:74
0.5	0.075	0.016	0.39	41:59
0.4	0.048	0.010	0.50	100:0
0.3	0.027	0.006	0.71	100:0

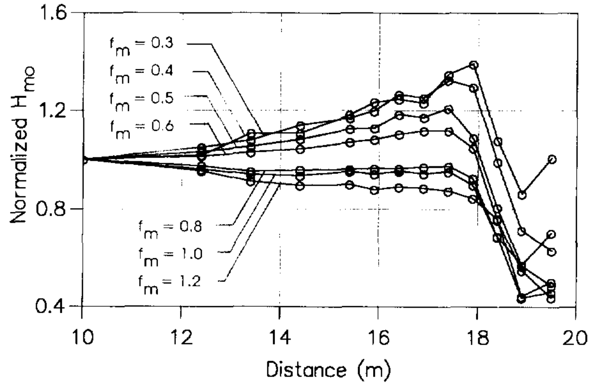

Fig. 2. Spatial evolution of the normalized H_{m0}. Measurements by Mase (1994), type WP2.

Hence the test cases considered by Mase (1994) cover both breaking regimes and it is to be expected that this will lead to rather different spatial evolutions of wave energy during the shoaling and breaking process. This is confirmed by Fig. 2, showing the variation of H_{m0} (normalized at WG1) for the different values of the mean frequency. A further analysis of the measurements shows that for decreasing values of the mean frequency, there is a gradual increase in low frequency motion and a pronounced increase in high frequency motion at the shoreline.

The wavemaker was controlled by a signal generated off-line using linear theory. Thus advanced features of compensation for generation of spurious sub-harmonics and super-harmonics as well as active absorption of free waves reflected from the slope was not included. Furthermore, the measured frequencies and amplitudes deviated slightly from the target. Altogether this prevents us from modelling the exact experimental setup and consequently we have chosen to place the numerical model boundary at the position of the first wave gauge (WG1) i.e. at the toe of the sloping beach. The energy on the primary frequencies and their super-harmonics propagates mainly onshore while sub-harmonic energy will propagate offshore as well as onshore. Neglecting the low frequency part of the incident waves, we use the following procedure: The measured signal at WG1 is analyzed by FFT, the low frequency motion is removed and the remaining signal is converted into a flux boundary condition using linear theory. At the position of WG1 the waves are generated internally and re-reflection from this boundary is avoided by using a 1 m wide sponge layer offshore from the line of generation. In order to resolve the super-harmonics in shallow water a grid size of 0.02 m and a time step of 0.01 s is used in the simulations.

Numerical simulations have been performed with bichromatic waves of type WP1 and WP2 for mean frequencies in the interval between 0.3 and 1.0 Hz. It is emphasized that all cases are simulated with the same set of standard model parameters (see part I, Section 2 for further details). The model results and the agreement with measurements are very similar for the two types of wave groups and only results from the case of WP2 will be shown here. Figs. 3–5 present measured and computed time series of water surface elevations at locations WG8, WG10 and WG12 and the motion of the shoreline

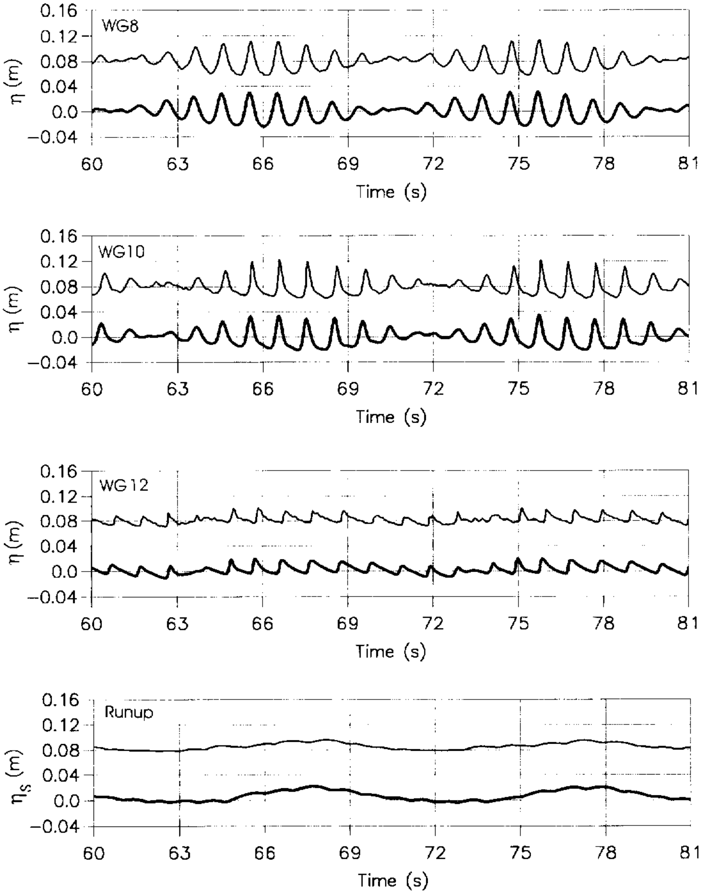

Fig. 3. Surface elevation (η) and swash oscillation (η_s, vertical displacement). Case: WP2, $f_m = 1.0$ Hz i.e. $f_1 = 1.05$ Hz and $f_2 = 0.95$ Hz. (————) Present model. (————) Experimental data by Mase (1994), shifted relative to computed results by 0.08 m.

converted into vertical displacement. For clarity, the measurements are shifted relative to the computational results by 0.08 m in the Figs. 3–5. The mean frequencies are 1.0 Hz in Fig. 3, 0.6 Hz in Fig. 4 and 0.3 Hz in Fig. 5 corresponding to surf zone conditions ranging from spilling to plunging breaking. Despite the variety in wave conditions the computed evolution of surface profiles and the resulting shoreline motion agree quite closely with the measurements, indicating that phenomena like dispersion, wave-wave interaction and dissipation due to breaking are well represented by the present model. The different wave conditions, ranging from spilling type to plunging type wave breaking, can be seen clearly in the shoreline motion: For the lower mean frequencies the individual swash of the primary waves is quite distinct at the shoreline, while in the case of higher mean frequencies the group induced sub-harmonic motion dominates the swash oscillations.

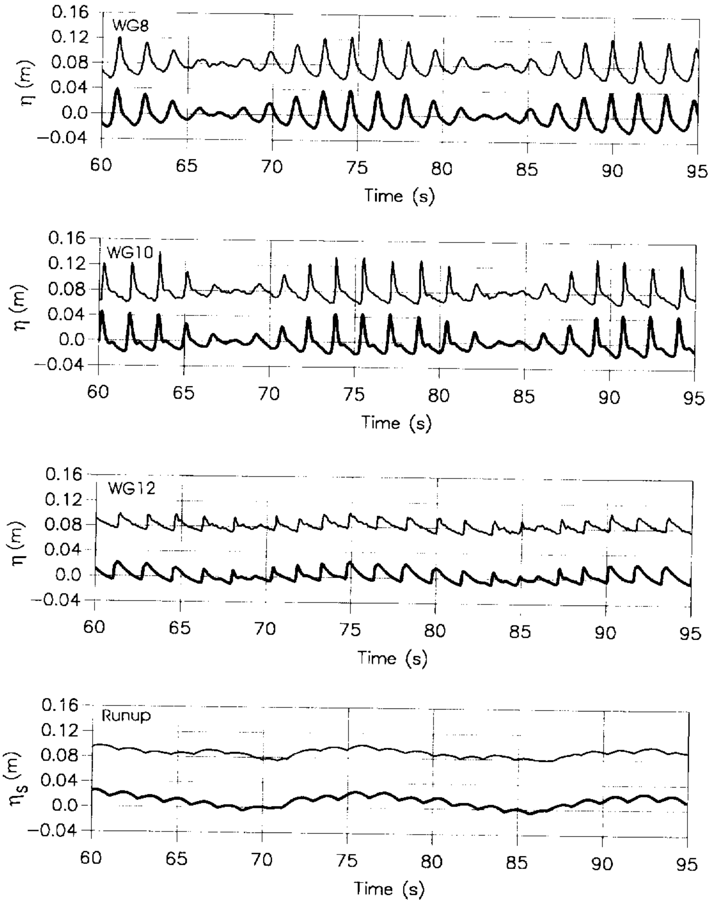

Fig. 4. Surface elevation (η) and swash oscillation (η_s, vertical displacement). Case: WP2, $f_m = 0.6$ Hz i.e. $f_1 = 0.63$ Hz and $f_2 = 0.57$ Hz. (———) Present model. (———) Experimental data by Mase (1994), shifted relative to computed results by 0.08 m.

It appears that the type of shoreline motion is governed by the type of wave breaking and consequently that the surf zone similarity parameter, ζ_0 can be used as an indicator. In order to test this assumption we focus on the test case of WP2 with $f_m = 0.3$ Hz. By changing the beach slope from 1/20 to 1/60 the value of ζ_0 will change from 0.71 to 0.24, indicating a change in wave breaker type from plunging to spilling. A more detailed analysis shows that on the 1/20 slope all waves will plunge while 86% of the waves (in the wave group) will be spilling on the 1/60 slope. The computed shoreline motions for the two beach slopes are shown in Fig. 6, where the time axis is shifted 16 s for the results on a beach slope of 1/60. The results clearly confirm our assumption: For a slope of 1/60 the individual swash has almost disappeared and the pattern of shoreline motion has become similar to the case of 0.8 Hz on a slope of 1/20. Hence we can

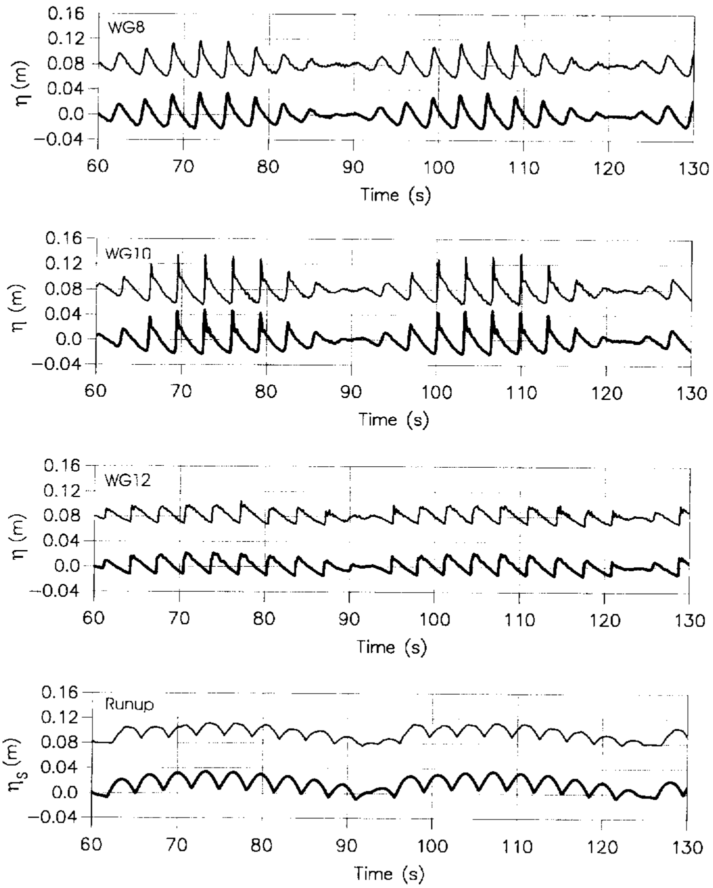

Fig. 5. Surface elevation (η) and swash oscillation (η_s, vertical displacement). Case: WP2, $f_m = 0.3$ Hz, i.e. $f_1 = 0.315$ Hz and $f_2 = 0.285$ Hz. (————) Present model. (————) Experimental data by Mase (1994), shifted relative to computed results by 0.08 m.

conclude that ζ_0 can be used to characterize the type of shoreline motion, and that plunging/surging breakers result in individual swash while spilling breakers result in low-frequency dominated shoreline motion.

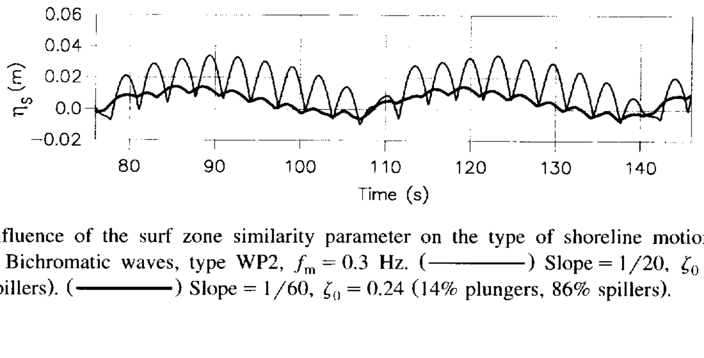

Fig. 6. The influence of the surf zone similarity parameter on the type of shoreline motion (η_s, vertical displacement). Bichromatic waves, type WP2, $f_m = 0.3$ Hz. (————) Slope = 1/20, $\zeta_0 = 0.71$ (100% plungers, no spillers). (————) Slope = 1/60, $\zeta_0 = 0.24$ (14% plungers, 86% spillers).

3.2. Irregular waves on a plane sloping beach and on a barred beach

Two cases of irregular waves are studied in this section involving a plane sloping beach and a barred beach.

The first case is based on the laboratory measurements reported by Cox et al. (1991) using the same flume as Mase (1994). The experimental setup is practically identical to what was described in Section 3.1 except for a few details: Only three wave gauges were applied and the experiments were repeated eleven times with the wave gauges moved to different locations along the slope. As a result 'simultaneous' measurements were obtained in still water depths of 47, 35, 30, 25, 20, 17.5, 15, 12.5, 10, 7.5 and 5 cm (denoted as WG1 to WG11). A target spectrum of Pierson–Moskowitz type with a peak frequency of 1.0 Hz and a significant wave height of 6.45 cm was considered. The surf

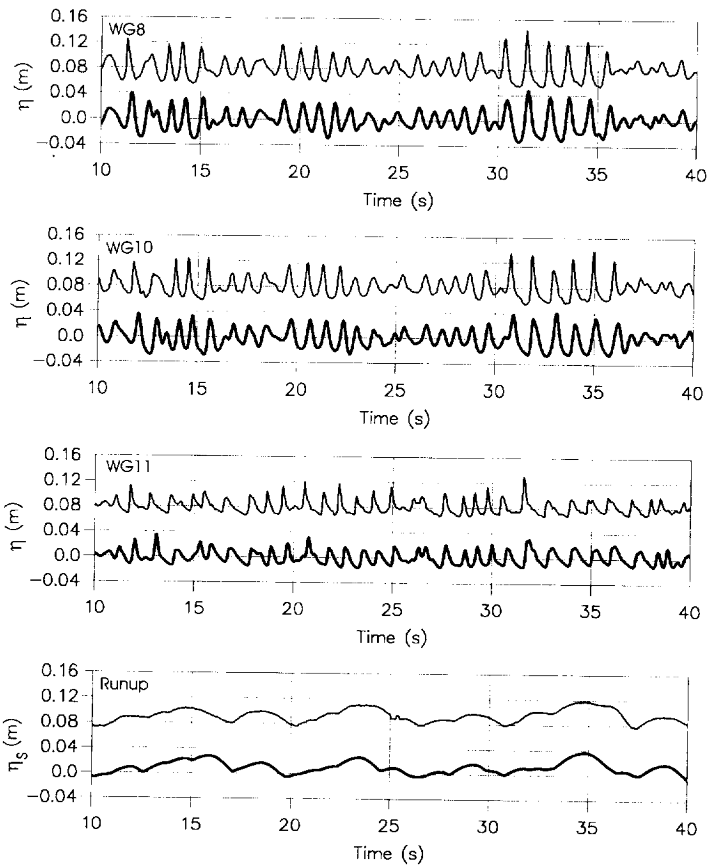

Fig. 7. Surface elevation (η) and swash oscillation (η_s, vertical displacement). Pierson–Moskowitz spectrum, $f_p = 1.0$ Hz. (———) Present model. (———) Experimental data by Cox et al. (1991), shifted relative to computed results by 0.08 m.

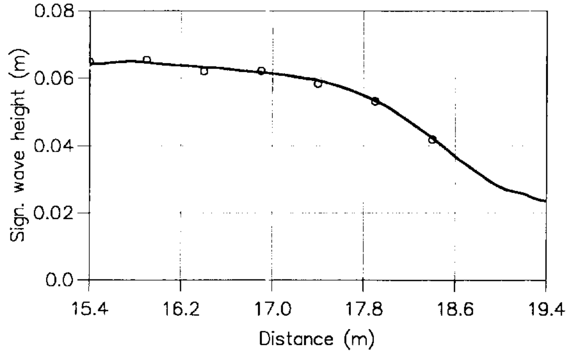

Fig. 8. Spatial variation of the significant wave height (H_{m0}). (———) Present model. (○) Experimental data by Cox et al. (1991).

similarity parameter was around 0.22 indicating spilling dominated type of wave breaking.

The Boussinesq model used in this study is restricted to h/L_0 values less than approximately 0.5 and beyond this value errors in the linear dispersion relation exceed 5% (see Madsen et al., 1991). Hence an accurate representation of free waves at 2.0 Hz (two times the peak frequency) requires the water depth to be less than 0.2 m.

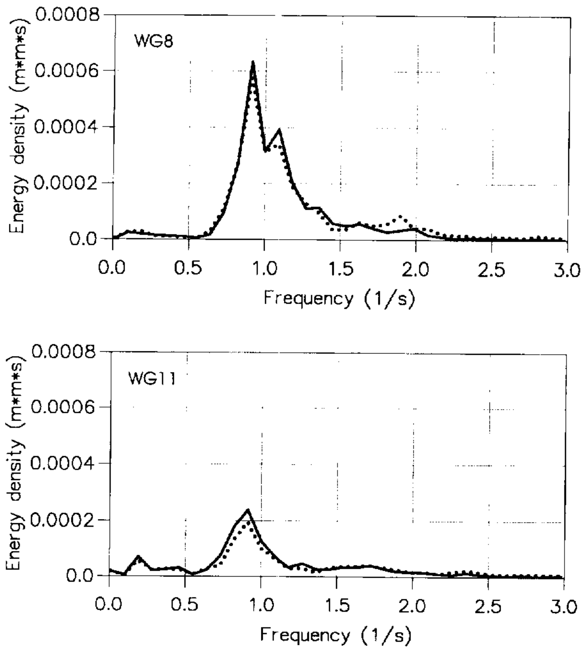

Fig. 9. Surface elevation spectra. (———) Present model. (· · ·) Experimental data by Cox et al. (1991).

Consequently we place the numerical model boundary at this depth (WG5) and follow the procedure described in Section 3.1: The measured surface elevation is analyzed by FFT, low frequency motion ($f < 0.1$ Hz) is removed and the remaining signal is converted into a flux condition. General model parameters are as described in Section 2 and the grid size and time step are as defined in Section 3.1.

Fig. 7 shows a comparison of surface elevations at locations WG8, WG10 and WG11. At these locations only minor discrepancies appear and generally the phases and amplitudes of the individual waves in the irregular wave train are accurately modelled. Also the computed shoreline motion converted into vertical displacement is in fairly good agreement with the measurements. It is seen to be dominated by low frequency oscillations, which is to be expected considering the low value of the surf similarity parameter. The variation of the significant wave height H_{m0} is shown in Fig. 8 to

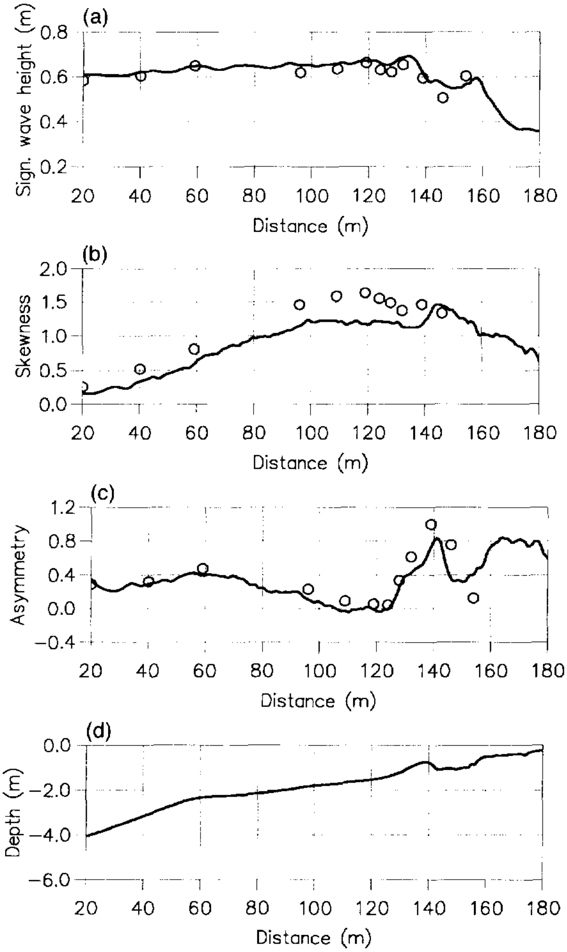

Fig. 10. Spectral measures of irregular waves on a barred beach. Spatial variation of (a) H_{m0}, (b) skewness, (c) asymmetry, (d) bathymetry. (————) Present model. (○) Experimental data by Arcilla et al. (1994).

compare well with measurements. The model also predicts the shape of the surface elevation spectra quite well, as shown in Fig. 9 for locations WG 8 ($x = 16.9$ m) and WG 11 ($x = 18.4$ m).

The second test case with irregular waves is based on the Delta Flume '93 laboratory experiment (Arcilla et al., 1994), which was conducted on a barred beach (Fig. 10d) using a Pierson–Moskowitz spectrum with peak frequency of 0.122 Hz and a significant wave height of 0.58 m. Fig. 10 shows the computed spatial variation of the significant wave height and of the skewness and asymmetry. The skewness and asymmetry are statistical measures of the wave form indicating deviations from symmetry about the horizontal and vertical axes, respectively (see Elgar and Guza, 1985). The skewness tends to be slightly underestimated by the model, but in general all three quantities agree quite well with the measurements outside as well as inside the two surf zones. The computed and measured asymmetries are both seen to grow strongly on the bar shoal, and to decay again in the bar trough. This indicates that the shapes of unbroken as well as broken waves are well represented by the time-domain model.

4. Surf beat and outgoing free long waves

In this section we concentrate on verifying the numerical model for low frequency waves generated and released in the surf zone. We shall base the study on bichromatic wave groups. While the experiments by Mase (1994, 1995) provided detailed results for the primary waves, they were not fine-tuned to give reliable results for the low-frequency motion. Complementary results can be found in Kostense (1984), who focused on a few low-frequency characteristics, but measured no details of the primary waves. He made an effort to control the wavemaker to get reliable results for the low-frequency motion.

Kostense presented flume tests of bichromatic waves breaking on a plane beach with emphasis on measuring the outgoing free long waves as being an important part of surf beat activity. The flume has a horizontal section of 40 m with a depth of 0.50 m and a 15 m section with a constant impermeable slope of 1/20. The experiments cover a range of primary frequencies, group frequencies, amplitudes and modulation rates. In the following we shall focus on test series A, B and E which study the effect of varying the group frequency for fixed values of the largest primary frequency f_1. The wave characteristics are listed in Table 2, which includes estimates of h/L_0, H_0/L_0 and ζ_0. Again L_0 is the deep water wave length based on the mean frequency, H_0 is the maximum wave height in the wave group (at deep water), h is the water depth taken at the toe of the slope and ζ_0 is the value of the surf similarity parameter based on H_0/L_0.

Table 2
Wave characteristics of experiments by Kostense (1984)

Series	f_1 (Hz)	Δf (Hz)	a_1 (m)	a_2 (m)	h/L_0	H_0/L_0	ζ_0
A	0.49	0.02–0.22	0.055	0.011	0.06	0.016	0.40
B	0.65	0.02–0.22	0.055	0.011	0.12	0.034	0.27
E	0.68	0.02–0.22	0.035	0.028	0.12	0.033	0.28

The magnitude of a_2/a_1 defines the modulation of the primary waves, which is weak in test series A and B and strong in test series E. The estimates of ζ_0 indicate spilling type wave breaking (for the highest waves) in all three test series, but using the more detailed analysis (as described in connection with Table 1) we find that all waves are spilling in test series A and B, while 81–85% of the waves are plungers in the highly modulated test series E.

The physical experiments were carried out with second order wave generation including correction for the bound long waves but neglecting the bound super-harmonics. This technique improved the stability of the incident nonlinear wave groups and significantly reduced the incidence of spurious free long waves. Additionally active wave absorption was applied to reduce the amount of re-reflection of long waves from the wave paddle. This technique resulted in high quality measurements and relatively stable wave conditions in the horizontal part of the wave flume.

The setup of the numerical model is slightly different from what was described in Section 3. Firstly the model boundary is placed 10 m from the toe of the slope. At this location bichromatic wave groups including second order sub-harmonics and super-harmonics are generated using the theory of Madsen and Sørensen (1993). The waves are generated inside the computational domain and re-reflection of short and long waves is avoided by the use of a 1 m wide absorbing sponge layer seaward of the point of generation. The grid size, the time step and other model parameters are identical to what was used in Section 3.

From the model results it can be concluded that it is not possible to generate completely stable wave groups and during the propagation over the horizontal part of the wave flume a gradual modulation of the low frequency wave appears. This confirms our previous experience with nonlinear bichromatic wave groups in shallow water: Although a second order boundary condition significantly reduces modulation of the sub-harmonic compared to a first order condition it does not completely eliminate the problem (see also Madsen and Sørensen, 1993).

This brings us to a discussion of the determination of the outgoing free long wave, which is generally complicated by the fact that the wave motion at the group frequency consists of three components, viz. the incident bound wave, the incident free wave and the reflected free wave. Splitting the low frequency signal into these three components requires recordings from three adjacent wave gauges. If, on the other hand the incident free wave can be neglected, the analysis simplifies and recordings from two adjacent wave gauges become sufficient. Finally a single wave gauge is sufficient if the incident free wave is neglected and the incident bound wave is estimated by the theoretical target value.

We have used both the three-point and the two-point analysis in the post-processing of the time series computed by the present numerical model. As expected the two point method is quite sensitive to the distance between the wave gauges and this has been varied gradually to produce fairly constant estimates in the horizontal part of the flume. Generally the two point analysis produces the most stable results, but it turns out that for a typical gauge distance of the order one tenth of a free long wave length the two methods lead to equivalent estimates of the outgoing free long wave. This indicates that the incident free long wave is negligible, although not totally absent. The model results

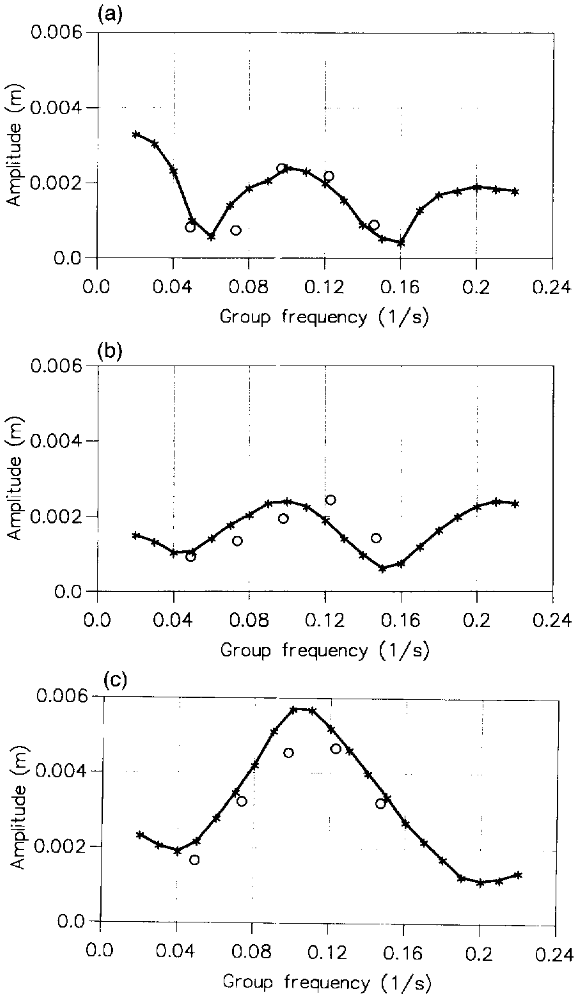

Fig. 11. Amplitude of free outgoing long wave against group frequency. (a) Test series A. (b) Test series B. (c) Test Series E. (————) Present model. (O) Experimental data by Kostense (1984).

presented in the following are all based on the two point analysis, which was also selected by Kostense (1984).

The computed amplitude of the outgoing free long wave is presented as a function of the angular frequency of the group in Fig. 11a–c for test series A, B and E, respectively. In case A the agreement with measurement is excellent with respect to shape as well as magnitude. In case B the magnitudes are also satisfactory, but the shape is slightly off compared to the measurements. In fact the same trend was found by Schäffer (1993) and Roelvink (1993) and we have no explanation for this discrepancy at present. In case E the shape is again in very good agreement with measurements, while the magnitudes are slightly overestimated by the model. In general it can be concluded that the model comparison with the experiments of Kostense (1984) is most satisfactory.

5. Further model investigations of surf beat

Having verified the numerical model on the evolution of surface elevations through the surf zone and on the resulting low frequency motion in the previous two chapters, we shall now concentrate on investigating special details of the surf beat mechanism. The following topics are addressed: trajectories of surface rollers, the motion of the breaker line and of the shoreline, the speed of breaking waves influenced by the surf beat, envelopes of surface elevations and their low-pass filtered components, change of wave group modulation through the surf zone, driving forces of low frequency motion inside and outside the surf zone, the influence of the group frequency on incoming bound long waves at the breakpoint, on the shoreline motion and on the outgoing free long waves for different modulation rates and bottom slopes.

For this investigation we shall concentrate on incident bichromatic wave groups which are effectively linear at the seaward boundary. This has the advantage that the determination of the amplitude of the outgoing free long waves due to the surf beat can be determined very accurately by simple means. The bathymetry used for this study consists of a horizontal part of 10 m with a depth of 1.2 m and a part with a constant sloping beach (various slopes are considered). The grid size, the time step and other model parameters are identical to what was used in Section 3. As wave input we use bichromatic wave groups as defined by Eqs. (3.1) and (3.2) with a fixed mean frequency $f_m = 0.60$ Hz, a fixed sum of amplitudes ($a_1 + a_2 = 0.08$ m), two different initial modulation rates, σ ($= a_2/a_1$) and a range of group frequencies (Δf) varying in the interval 0.02–0.14 Hz. In all tests waves are generated inside the model domain and re-reflection from the offshore boundary is avoided by using a sponge layer seawards of the point of generation.

In the first test case the beach slope is $h_x = 1/40$, the still water shoreline is at $x = 58$ m, while two wave groups with $\sigma = 0.2$ and $\sigma = 1.0$ are considered. As mentioned above, the sum of a_1 and a_2 at the point of wave generation is constant which implies that the highest waves in each of the two wave groups are of equal size. Hence we may expect that the outermost breakpoint position, $x_{B,outer}$ will be almost the same for the two wave groups, while the innermost breakpoint, $x_{B,inner}$ will be quite different as it is determined from the smallest waves in the wave group. This is confirmed by Fig. 12a–b, which shows the computed trajectories of the surface rollers (represented by tracking the steepest point of the wave fronts) and the shoreline motion for a group frequency $\Delta f = 0.02$ Hz in which case the group motion is resolved by 30 mean periods. We notice that $x_{B,outer}$ is practically identical for the two modulation rates, while $x_{B,inner}$ depends strongly on σ. The breakpoint excursion between these two limits is seen to be well resolved by the number of rollers being detected and traced. The almost sinusoidal time-variation of x_B for $\sigma = 0.2$ is significantly distorted as the modulation is increased to $\sigma = 1.0$, the reason being that $x_B(t_2) = x_{B,inner}$ is delayed relative to $x_B(t_1) = x_{B,outer}$ with half a group period *plus* the travelling time necessary

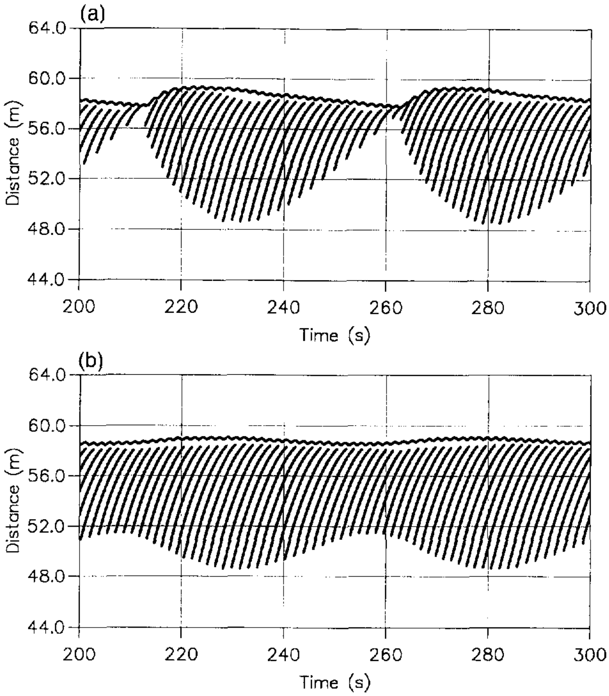

Fig. 12. Trajectories of surface rollers and shoreline motion. Group frequency, $\Delta f = 0.02$ Hz. Bottom slope $= 1/40$, $f_m = 0.60$ Hz, $f_1 = f_m + \Delta f/2$, $f_2 = f_m - \Delta f/2$; $a_1 + a_2 = 0.080$ m. (a) Modulation rate, $a_2/a_1 = 1.0$; (b) modulation rate, $a_2/a_1 = 0.2$.

for the lowest waves to cover the distance from $x_{B,outer}$ to $x_{B,inner}$. This delay was also discussed by Symonds et al. (1982). In Fig. 13a–b the group frequency is increased to $\Delta f = 0.05$ Hz. Apparently this leads to a small shorewards shift of $x_{B,outer}$ and a seawards shift of $x_{B,inner}$ leading to a minor reduction in the breakpoint excursion for both modulation rates. It turns out that this trend is amplified for increasing ratios of the group frequency to the mean frequency $(\Delta f/f_m)$ and when this number is larger than say $1/3$ the effective excursion produced by the model almost vanishes.

The shoreline excursion in Figs. 12 and 13 is seen to be dominated by low frequency motion while the individual bores almost vanish. The fully modulated case obviously results in the strongest motion, as would be expected from both second order theory for bound waves and from the theory of the generating mechanism due to breakpoint oscillations. The non-sinusoidal variation of the breakpoint position is also found in the breakpoint forcing and thereby in the surf beat motion. Thus (in Fig. 12aFig. 13a) the shape of the resulting shoreline motion indicates substantial energy on harmonics of the group frequency i.e. $2\Delta f$, etc.

The steepness of the trajectories of the rollers indicates the local speed of the breaking waves and especially close to the shoreline this is clearly influenced by the low frequency motion. As discussed in part I (Section 2.4) the wave celerity used by the

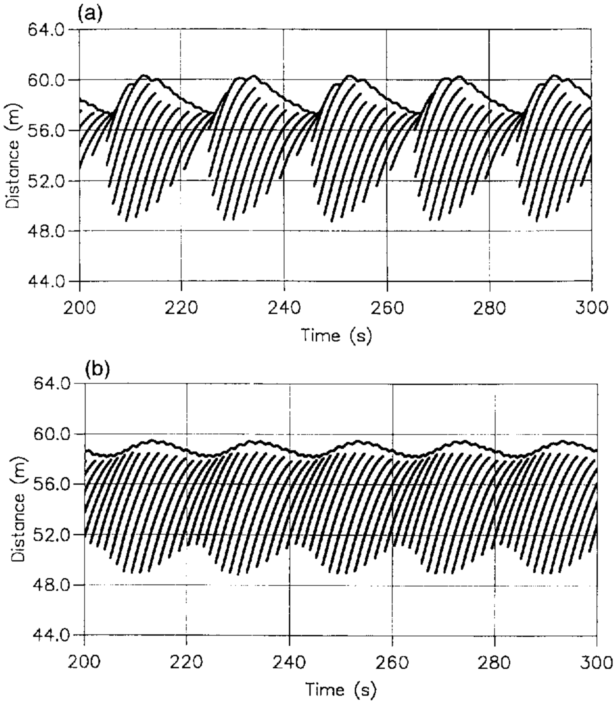

Fig. 13. Trajectories of surface rollers and shoreline motion. Group frequency, $\Delta f = 0.05$ Hz. Otherwise as Fig. 12. (a) Modulation rate, $a_2/a_1 = 1.0$; (b) modulation rate, $a_2/a_1 = 0.2$.

roller model is not determined directly from the trajectories but from spatial and temporal derivatives of the surface elevation taken at the steepest point of the wave front. Fig. 14 shows the temporal variation of the bore speed determined by tracing eleven specific surface rollers for the fully modulated case from Fig. 13a. The results (shown as full lines) are compared to the empirical wave celerity

$$c = 1.3\sqrt{gh} \tag{5.1}$$

where h is the still water depth. Note that Eq. (5.1) was used in the earliest versions of the model (as reported by Schäffer et al., 1993) and that Eq. (5.1) has proved to be acceptable for regular waves (see part I, Fig. 2). However, Fig. 14 clearly shows that this formula fails in connection with irregular waves, in which case the low frequency motion has a clear influence on the speed of the individual bores. During the period from the minimum to the maximum run-up, where the low frequency motion is directed onshore the speed of the bores is seen to be considerably larger than indicated by Eq. (5.1), while the opposite occurs when the low frequency motion is directed offshore.

The modulation of the wave groups changes slightly during the processes of shoaling and nonlinear interactions, but much more rapid variations can be expected in the surf zone. In numerical modelling this obviously depends on the type of breaker model applied and as an example the classical assumption of a saturated surf zone (with wave

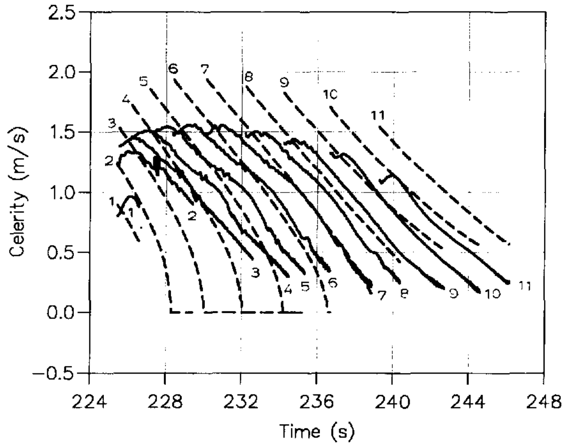

Fig. 14. Temporal variation of wave celerity (tracking eleven rollers during a group period). $\Delta f = 0.05$ Hz, $a_2/a_1 = 1.0$. Otherwise as Fig. 12. (————) Interactively determined numerical celerity. (- - -) Approximation using Eq. (5.1).

amplitudes proportional to the local water depth) leads to a vanishing modulation. Schäffer (1993), on the other hand discussed the possibility of a reversion of modulation and such a reversion is indeed possible in the present model, because of the difference between the initial limiting breaker angle for non-breaking waves (20°) and the final breaker angle (10°) for waves already breaking (see Section 2, part I). We shall investigate the change of modulation predicted by the present model in the following Figs. 15–17.

Fig. 15 shows the spatial variation of the maximum and minimum surface elevations (crest and trough envelope) obtained during the last two wave groups of the simulation (for the case of $\sigma = 1.0$ and $\Delta f = 0.05$ Hz). The figure also contains an instantaneous

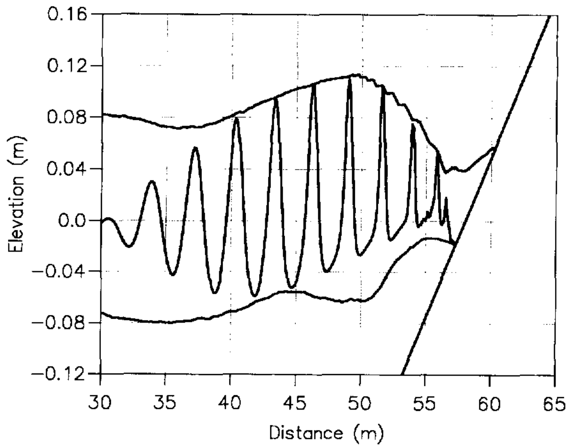

Fig. 15. Spatial variation of surface elevation and envelope of crest and trough variations. $\Delta f = 0.05$ Hz, $a_2/a_1 = 1.0$. Otherwise as Fig. 12.

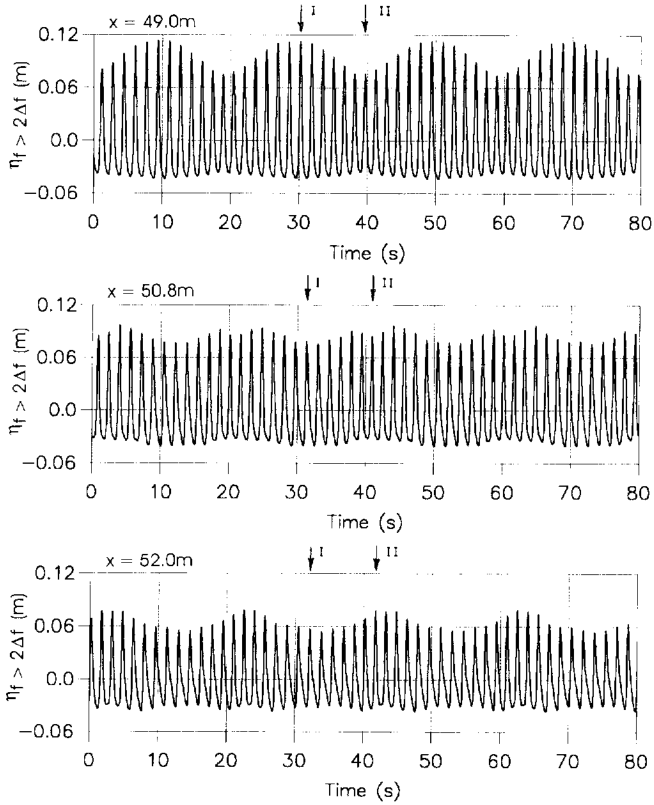

Fig. 16. Time series of computed high-pass filtered ($f > 2\Delta f$) surface elevations at three locations. $\Delta f = 0.05$ Hz, $a_2 / a_1 = 0.2$. Otherwise as Fig. 12.

picture of the surface elevations shown at an instant when the crest envelope is reached in the surf zone. The individual waves can be seen to steepen and break in shallow water. Half a group period later the surface elevation will reach the trough envelope in

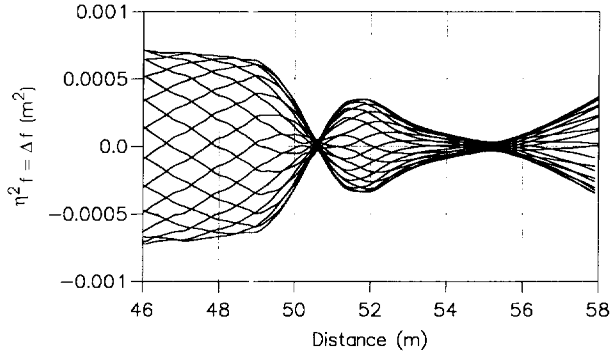

Fig. 17. Spatial variation and envelope of $\eta^2_{f=\Delta f}$, band-pass filtered square of surface elevations. $\Delta f = 0.05$ Hz, $a_2 / a_1 = 0.2$. Otherwise as Fig. 12.

the surf zone and we notice that the low frequency component of the surface elevation is significant indicating that the surf beat has a major influence on the breaking process. The crest envelope has several small but distinct spikes indicating a number of different breakpoint positions: The outermost spike is established when the highest waves reach their limiting steepness and start breaking. This is followed by a clear decay in the envelope. The second spike occurs when the second highest waves shoal to become higher than the waves already breaking. This process is repeated for all the waves in the wave group indicating a gradual change of modulation.

Further evidence of the change of modulation during breaking is presented in Fig. 16 which shows high-pass filtered timeseries of computed surface elevations at three locations for the case of $\sigma = 0.2$ and $\Delta f = 0.05$ Hz. The high-pass filtering ($f > 2\Delta f$) makes it easier to spot the modulation of the primary waves without the influence of the low frequency motion. At $x = 49$ m the highest waves have just started breaking and the modulation is similar to the input wave train. At $x = 50.8$ m the former highest waves (indicated by I) have been reduced by breaking and are now approximately of the same size as the former lowest waves (indicated by II). Hence the modulation has almost vanished at this location. At $x = 52$ m a relatively strong reversion of modulation has occurred and the former highest waves are now the lowest waves in the wave group. A similar trend can actually be observed in the fully modulated experimental data of Mase (1994), which were used for verification in Section 3.1. We can therefore conclude that the reversion is not just an artifact of the numerical model.

Another way of illustrating the change of modulation is to compute the quantity $\eta^2_{f=\Delta f}$ which is determined as the square of the surface elevation followed by a band-pass filtering to allow for motion on the group frequency only. This function is proportional to the product of the local amplitudes at the two primary frequencies and therefore also sensitive to the modulation. Fig. 17 shows the spatial variation of $\eta^2_{f=\Delta f}$ computed for the case of $\sigma = 0.2$ and $\Delta f = 0.05$ Hz (the corresponding surface roller trajectories were shown in Fig. 13b). We notice that the envelope of $\eta^2_{f=\Delta f}$ is decreasing steeply from $x = 49$ m (i.e. the outermost breakpoint) to $x = 50.8$ m, where a nodal point occurs due to the vanishing modulation. Beyond this point the modulation is reversed and increasing, a mechanism which will tend to increase the envelope of $\eta^2_{f=\Delta f}$. The general decay of wave amplitudes due to breaking will, however, have a counteracting effect and as a result a local maximum of $\eta^2_{f=\Delta f}$ is found at $x = 51.8$ m. Repeating the above procedure for other values of the initial modulation (σ) and the group frequency (Δf) leads to figures similar to Fig. 17, with virtually no influence from changes in Δf. An increase in σ, however has the following effect: Outside the breaking zone $\eta^2_{f=\Delta f}$ will increase in proportion to $\sigma/(1+\sigma)^2$, while inside the breaking zone the position of the nodal point in $\eta^2_{f=\Delta f}$ tends to move shorewards in agreement with the similar shift of the innermost breakpoint.

The radiation stress gradient inherent in the Boussinesq equations of the present model can be determined by time-averaging the nonlinear momentum term (see Section 4.2, part I), which reads

$$N \equiv -\rho \frac{\partial}{\partial x}\left(\frac{1}{2} g \eta^2 + \frac{P^2}{d} + R \right) \tag{5.2}$$

where P is the depth-integrated velocity (volume flux), d is the total water depth and R is the excess momentum due to the surface rollers. Note that R may either be regarded as part of the radiation stress (as done here) or as a separate excess momentum contribution (as done in part I). A first estimate to Eq. (5.2) can be obtained by neglecting the R-term and approximating the P-term by $g\eta^2$. This yields

$$N \approx -\frac{3}{2}\rho g \frac{\partial}{\partial x}(\eta^2) \tag{5.3}$$

which shows the importance of the quantity $\eta^2_{f=\Delta f}$ considered above. Note that in shallow water, Eq. (5.3) is consistent with the formulations used by Symonds et al. (1982), Roelvink et al. (1992) and Schäffer (1993). In the present application considering bichromatic wave groups we determine the slowly varying radiation stress gradient (including the roller effect) by computing the time variation of N (as defined by Eq. (5.2)) and taking the band pass filter of the result. The result, denoted by $N_{f=\Delta f}$, is the driving force of the oscillatory low frequency motion and it contains the local forcing of bound long waves as well as the effect of the oscillating break point, two mechanisms which can not be separated in the present approach. The steady component of N, which is responsible for the average setup of the mean water level is not included in $N_{f=\Delta f}$. Fig. 18 shows the spatial variation of $N_{f=\Delta f}$ determined for the case of $\sigma = 0.2$ and $\Delta f = 0.05$ Hz. We notice that $N_{f=\Delta f}$ has a global maximum at $x = 51.5$ m, a local minimum at $x = 52.5$ m and yet another local maximum at $x = 53.0$ m. In case the radiation stress gradient had been approximated by Eq. (5.3) the maximum generation would occur at $x = 50.8$ m which is the nodal point for $\eta^2_{f=\Delta f}$ (Fig. 17), while a local minimum would occur at $x = 51.8$ m where the effect of increasing reversed modulation balances the effect of decaying amplitudes. These expected positions have been shifted shorewards in Fig. 18 by 0.7 m, a typical result of including the roller momentum term R (see also Section 4.2, part I). Repeating the above procedure for other values of the initial modulation and the group frequency we arrive at the following conclusions: Inside the surf zone the forcing has two distinct peaks separated by a local minimum which moves shorewards for increasing values of σ. For σ approaching unity the second peak disappears and the forcing becomes more evenly distributed. This can be

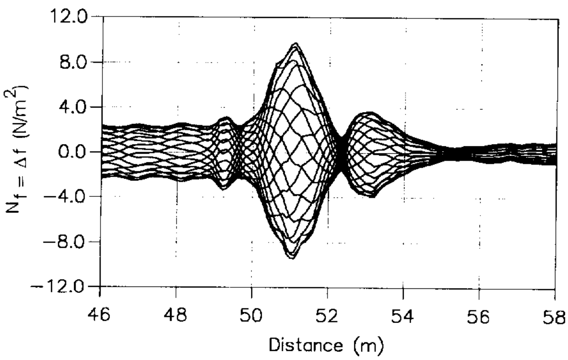

Fig. 18. Spatial variation and envelope of $N_{f=\Delta f}$, band-pass filtered radiation stress gradient determined from Eq. (5.2). $\Delta f = 0.05$ Hz, $a_2/a_1 = 0.2$. Otherwise as Fig. 12.

understood, since the breakpoint for fully modulated incident waves will tend to oscillate over the whole surf zone smearing out the breakpoint forcing. However, the global maximum in the forcing always occurs just inshore of the outermost breakpoint and the peak value as well as the position of it turns out to be almost independent of Δf and σ. Outside the surf zone the forcing increases for increasing values of σ and Δf, consistent with a similar variation in the amplitude of the incoming bound long waves as will be discussed below in connection with Fig. 20.

The combination of bound and free long waves resulting partly from the direct forcing by $N_{f=\Delta f}$ and partly from the shoreline reflection of long waves is determined as $\eta_{f=\Delta f}$ i.e. by band-pass filtering the computed surface elevation at the group frequency. This computation excludes the stationary setup of the mean-water level. The resulting surf beat is shown for two group frequencies using $\Delta f = 0.08$ Hz in Fig. 19a and $\Delta f = 0.05$ Hz in Fig. 19b ($\sigma = 0.2$). These frequencies correspond to a local minimum and maximum, respectively for the amplitude of the outgoing long wave, as shown below (Fig. 22).

We shall now turn to an investigation of the surf beat sensitivity to bottom slope, modulation rate and group frequency with emphasis on the incoming bound long waves

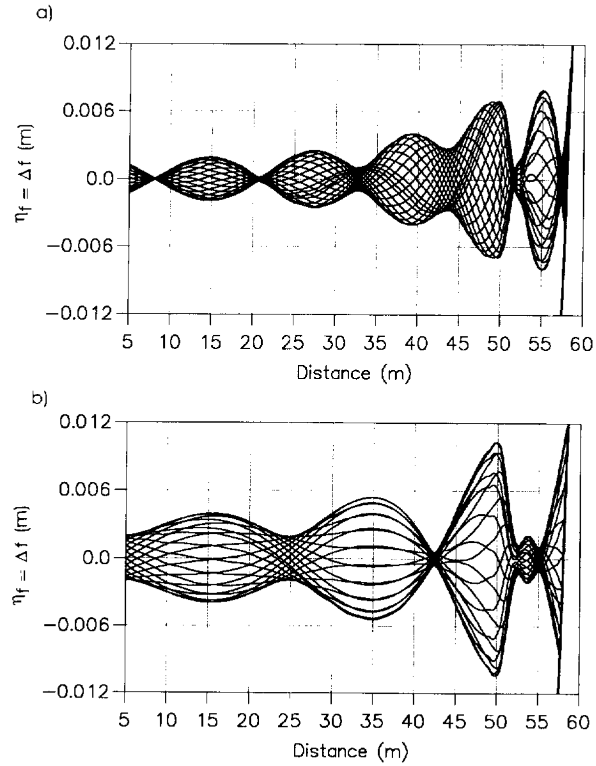

Fig. 19. Spatial variation and envelope of $\eta_{f=\Delta f}$, band-pass filtered surface elevations. $a_2/a_1 = 0.2$. Otherwise as Fig. 12. (a) $\Delta f = 0.08$ Hz, (b) $\Delta f = 0.05$ Hz.

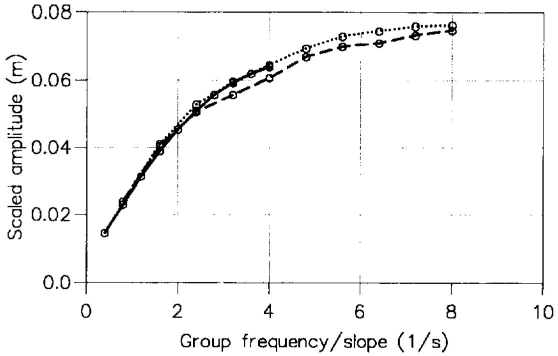

Fig. 20. Amplitude of bound long waves determined at $h = h_{B,outer}$ and scaled with $\sigma/(1+\sigma)^2$, where $\sigma = a_2/a_1$. Solution to complex amplitude evolution equations (Madsen and Sørensen, 1993). Wave input: $f_m = 0.60$ Hz, $f_1 = f_m + \Delta f/2$, $f_2 = f_m - \Delta f/2$; $a_1 + a_2 = 0.080$ m. (———) $a_2/a_1 = 1.0$, $h_x = 1/20$; (---) $a_2/a_1 = 0.2$, $h_x = 1/40$; (· · ·) $a_2/a_1 = 1.0$, $h_x = 1/40$.

at the breakpoint, the shoreline motion and the resulting outgoing free long waves (Figs. 20–23). Second order theory (valid on a horizontal bottom) predicts that the long waves bound to the incoming wave groups will be proportional to the product of a_1 and a_2, which indicates a scaling of $\sigma/(1+\sigma)^2$, i.e. they will be almost twice as large with $\sigma = 1.0$ as compared to $\sigma = 0.2$. In shallow water the theory also predicts the bound long waves to be independent of the group frequency for a fixed mean frequency. However, on a sloping bottom the bound long waves do not have the time (or distance) to build up to the size of the local constant-depth solution. In order to estimate the bound long waves in the vicinity of the outermost breakpoint we have solved the Boussinesq equations recast into a set of complex evolution equations as described by Madsen and Sørensen (1993). By this procedure reflections and effects of wave breaking are absent and the incoming bound long waves can be explicitly determined. The position of the breakpoint, $x_{B,outer}$ is determined from the present numerical time-domain model and the

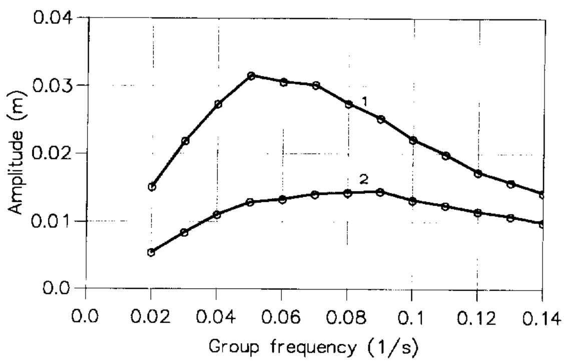

Fig. 21. Shoreline motion (vertical displacement) as a function of modulation and group frequency. Bottom slope, $h_x = 1/40$. Wave input as Fig. 20. (1) $a_2/a_1 = 1.0$; (2) $a_2/a_1 = 0.2$.

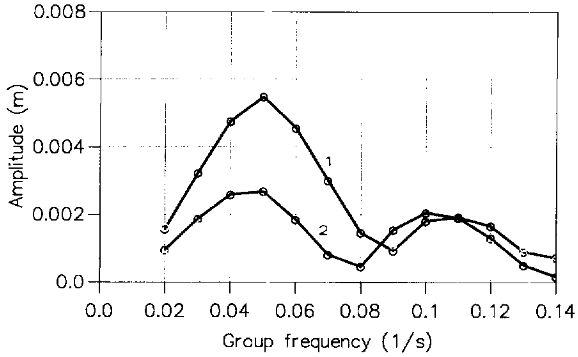

Fig. 22. Amplitude of outgoing free long wave as a function of modulation and group frequency. Bottom slope, $h_x = 1/40$; Wave input as Fig. 20. (1) $a_2/a_1 = 1.0$; (2) $a_2/a_1 = 0.2$.

results from the evolution equations are presented at this position. Computations are made for a range of group frequencies and for three different combinations of the modulation rate (σ) and the bottom slope (h_x), while the mean frequency (f_m) and the maximum incident wave amplitude ($a_1 + a_2$) are kept constant as mentioned previously. Hence, $h_{B,outer}$, the depth at the point of breaking will be practically constant for the various solutions. Fig. 20 shows the resulting amplitude (a_b) of the bound long wave at $h_{B,outer}$ scaled with the factor $(1+\sigma)^2/\sigma$, while $\Delta f/h_x$ is used as abscissa as inspired by the solution of Schäffer (1993) (for a simple one-way energy transfer) depending on the parameter $h_x f_m/\Delta f$. We notice that all curves in Fig. 20 practically coincide and we can conclude that the main variation with σ, Δf and h_x has been absorbed in the scaling of the axes and that the amplitude of the bound long waves at the breakpoint increase significantly for increasing values of σ and Δf and for decreasing h_x. This trend is in agreement with the variation of the radiation stress forcing outside the surf zone as discussed in connection with Fig. 18.

Returning to the results obtained by the present time-domain model, Fig. 21 summarizes the computed amplitudes of the shoreline motion as a function of the group

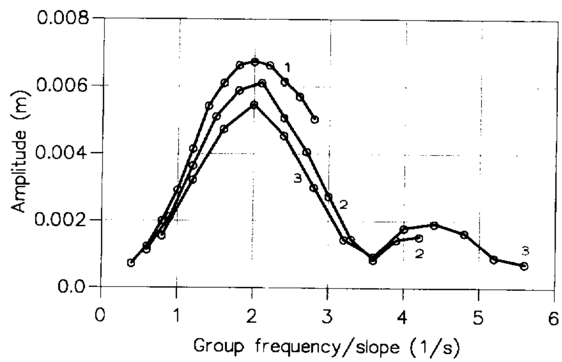

Fig. 23. Amplitude of outgoing free long wave as a function of group frequency over bottom slope ($\Delta f/h_x$). Full modulation ($a_2/a_1 = 1.0$); wave input as Fig. 20. (1) $h_x = 1/20$; (2) $h_x = 1/30$; (3) $h_x = 1/40$.

frequency. We notice a (local) maximum at $\Delta f \approx 0.05$ (for $\sigma = 1.0$) and at $\Delta f \approx 0.09$ (for $\sigma = 0.2$). The amplitude is seen to decrease for larger values of Δf, which is somewhat surprising in view of Fig. 20 revealing a continuous growth of bound long waves at the breakpoint. It turns out, however, that the reflection of long waves at the shoreline gradually decreases for increasing Δf. The reason is partly physical and partly numerical: from a physical point of view one may expect that the individual rollers connected with the short waves may also have a dissipative effect on the long waves when the difference in scaling (i.e. $f_m/\Delta f$) is decreased. From a numerical point of view the combination of the scheme and the special treatment of the shoreline will be increasingly dissipative for higher group frequencies in the swash zone. Further research (experimental and numerical) of swash zone dynamics for higher group frequencies is necessary in order to quantify the reliability of the numerical model in this regime.

Fig. 22 shows the computed amplitudes of the outgoing free long wave determined on the horizontal section seawards from the surf zone. The curve is seen to oscillate with the group frequency, a trend which is in qualitative agreement with the theory of Symonds et al. (1982), who showed the importance of the relative phase between the long waves reflected from the shoreline and the long waves directly generated in the seawards directions by the moving breakpoint mechanism. Their theory predicts a minimum response at $\chi = 3.67$, 12.31, etc., corresponding to maxima of the linear standing wave solution $J_0(2\sqrt{\chi})$, where J_0 is the Bessel function of order zero and χ is defined by

$$\chi \equiv \frac{(2\pi\Delta f)^2 \overline{h_B}}{g h_x^2} \tag{5.4}$$

with $\overline{h_B}$ being the depth at the average breakpoint position. In the computations shown in Fig. 22 (for $\sigma = 0.2$) the value of $\overline{h_B}$ is approximately 0.2 m independently of Δf and the computed minimum occurring at $\Delta f = 0.08$ Hz correspond to a χ-value around 8, which is much higher than the prediction of Symonds et al. This trend is, on the other hand supported by the measurements of Kostense (1984) as well as by the analytical work of Schäffer (1993). It is therefore likely that the deviation from the prediction of Symonds et al. is due to their omission of the incident bound long waves. Fig. 22 also shows than when σ is increased to 1.0 the local minima occur for slightly higher values of Δf. This may be explained by the χ-scaling as the average position of the breakpoint is closer to the shoreline for the larger modulation rates. Another obvious trend is that the local maxima decrease for increasing group frequencies. This is connected with the overall decrease in the shoreline motion as seen in Fig. 21.

Finally, Fig. 23 summarizes the computed amplitudes of outgoing free long waves for a range of group frequencies, full modulation ($\sigma = 1.0$) and three bottom slopes (1/20, 1/30, 1/40). The abscissa is now $\Delta f/h_x$ inspired by the definition of χ and the position of the local extrema coincide. The peak values in Fig. 23 tend to grow for larger values of the bottom slope, and as the amplitude of the bound long waves at the breakpoint is independent of $\Delta f/h_x$ (see Fig. 20) this effect is due to differences in the oscillating breakpoint generating mechanism and perhaps also to differences in shoreline reflection and long-wave dissipation.

In conclusion, the different aspects of surf beats as modelled here are in qualitative agreement with the analytical model of Schäffer (1993). At one point, though, there is a difference and that is the question of whether the long-wave activity generally increases or decreases for increasing group frequency. The reason for this discrepancy appears to be related to long-wave dissipation and partial reflection inherent in the present model as compared with Schäffers simplification of no dissipation and full reflection of long waves. Hopefully, future experiments will reveal to which extent these effects are physical phenomena rather than numerical artifacts.

6. Summary and conclusion

In this paper cross-shore wave motion in the surf zone has been considered including shoaling, breaking and runup of bichromatic wave groups and irregular waves, and the resulting generation of surf beats. These phenomena have been investigated numerically by using a time-domain Boussinesq type model, which resolves the primary wave motion as well as the long waves. Mutual interaction between short waves and long waves is inherent in the model. This allows for a general exchange of energy between triads rather than a simple one-way forcing of bound waves as well as a substantial modification of bore celerities in the swash zone due to the presence of long waves.

As compared with the classical Boussinesq equations the ones adopted here allow for improved linear dispersion characteristics and wave breaking is incorporated by using a surface roller concept. The swash zone is included by incorporating a moving shoreline boundary condition and radiation of short and long period waves from the offshore boundary is allowed by the use of absorbing sponge layers. It is emphasized that all model simulations presented in this paper (part II) are conducted with the same default set of parameters defining the breaker model and the shoreline model. These parameters are described and specified in part I, see Madsen et al. (1997).

In Section 3.1 we have verified the model against the experimental data of Mase (1994) considering breaking and runup of fully modulated bichromatic wave groups on a gently sloping beach. While the ratio of the group frequency to the mean frequency is kept constant throughout the test series, the mean frequency is varied to produce a range of different breaker types. For the highest mean frequencies all waves are spilling whereas plunging breakers dominate for the lowest mean frequencies. Computed and measured surface elevations have been compared at a number of locations outside and inside the surf zone and the agreement is generally very good.

The same conclusion applies to the shoreline oscillations. These generally consist of a significant low frequency component at the group frequency and individual swash of the primary waves. For the Mase experiments with low values of the mean frequency (plunging breakers) the individual swash tends to dominate the shoreline motion, while the low frequency motion dominates when the mean frequency is higher (spilling breakers). This trend has been reproduced very accurately by the Boussinesq model and the agreement in shoreline motion is very good in all the test series. In order to investigate whether the type of shoreline motion can be classified by the surf similarity parameter (ζ_0), we have repeated one of the simulations with a bottom slope being three times milder than the one used in the Mase experiments. This reduces ζ_0 from the plunging regime to the spilling regime, and the computed shoreline motion behaves accordingly: The swash of the individual bores almost vanish on the milder bottom slope.

Breaking and runup of irregular wave trains has been studied in Section 3.2. The model is verified against the laboratory experiments of Cox et al. (1991) and Arcilla et al. (1994) with emphasis on timeseries of surface elevations at fixed locations outside and inside the surf zone, time series of the shoreline motion, and spectral measures such as the spatial variation of the significant wave height, the skewness and the asymmetry. It can be concluded that the model captures the evolution of wave profiles through the surf zone quite well.

In Section 4 we have concentrated on the classical surf beat experiments by Kostense (1984), who considered breaking and runup of bichromatic wave groups and studied the effect of varying the group frequency for fixed values of the largest primary frequency, f_1. Three test series are simulated (A, B and E) characterized by slightly different values of f_1 and including two different modulation rates (0.2 and 0.8). The results are represented by the amplitude of the outgoing free long wave as a function of the group frequency. The model results are generally in good agreement with the measurements of Kostense.

Finally in Section 5, we have studied special mechanisms in the surf beat phenomenon on the basis of bichromatic wave groups. This includes e.g. the motion of the breaker line, which is identified from trajectories of surface rollers, the slowly varying radiation stress gradient, which is forcing bound long waves, as well as the breakpoint generated waves, and the influence of long waves on the celerity of the individual bores. The chapter also includes computed envelopes of crest and trough elevations and envelopes of low frequency motion. Computations are made for a fixed mean frequency and for a range of group frequencies, two modulation rates and three bottom slopes. It is emphasized that the results obtained in this section are mainly qualitative due to the lack of experimental data. Hopefully, future high quality laboratory experiments can provide details necessary for further verification.

Acknowledgements

This work has been financed by the Danish National Research Foundation and their support is greatly appreciated. Many thanks are due to Dr. Hajime Mase from Kyoto University for making his raw experimental data for swash oscillations available to us.

References

Arcilla, A.S., Roelvink, J.A., O'Connor, B.A., Reniers, A., Jimenez, J.A., 1994. The Delta flume '93 experiment. Proc. Coastal Dynamics Conf., UPC, Barcelona, pp. 488–502.

Battjes, J.A., 1974. Surf similarity. In: Proc. of the 14th Coastal Eng. Conf. ASCE, pp. 466–480.

Battjes, J.A., Janssen, J.P.F.M., 1978. Energy loss and set-up due to breaking of random waves. In: Proc. 16th Int. Conf. Coastal Eng. ASCE, pp. 569–587.

Cox, D.T., Mase, H., Sakai, T., 1991. An experiment on the effect of fluid acceleration on seabed stability. Report No. 91-HY-01. Kyoto University, Japan.

Elgar, S., Guza, R.T., 1985. Observations of bispectra of shoaling surface gravity waves. J. Fluid Mech. 161, 425–448.

Freilich, M.H., Guza, R.T., 1984. Nonlinear effects on shoaling surface gravity waves. Philos. Trans. R. Soc. London A 311, 1–41.

Galvin, C.J. Jr., 1968. Breaker type classification on three laboratory beaches. J. Geophys. Res. 73 (12), 3651–3659.

Kostense, J.K., 1984. Measurements of surf beat and set-down beneath wave groups. In: Proc. of the 19th Coastal Eng. Conf. pp. 724–740.

Van Leeuwen, P.J., 1992. Low frequency wave generation due to breaking wind waves. Ph.D. thesis. Delft University, 150 pp.

List, J.H., 1992. A model for the generation of two-dimensional surf beat. J. Geophys. Res. 97 (C4), 5623–5635.

Lo, J.-M., 1988. Dynamic wave setup. In: Proc. of the 21th Coastal Eng. Conf. ch. 74, pp. 999–1010.

Longuet-Higgins, M.S., Stewart, R.W., 1962. Radiation stress and mass transport in gravity waves with application to 'surf beats'. J. Fluid Mech. 13, 481–504.

Madsen, P.A., Murray, R., Sørensen, O.R., 1991. A new form of the Boussinesq equations with improved linear dispersion characteristics. Coast. Eng. 15, 371–388.

Madsen, P.A., Sørensen, O.R., 1993. Bound waves and triad interactions in shallow water. Ocean Eng. 20, 359–388.

Madsen, P.A., Schäffer, H.A., Sørensen, O.R., 1997. Surf zone dynamics simulated by a Boussinesq type model. Part I: Model description and cross-shore motion of regular waves. Coast. Eng. 32, 255–288.

Mase, H., 1994. Uprush–backrush interaction dominated and long wave dominated swash oscillations. In: Proc. of Int. Symposium: Waves – Physical and Numerical Modelling. Vancouver, Canada, pp. 316–325.

Mase, H., 1995. Frequency down-shift of swash oscillations compared to incident waves. J. Hydraulic Res. 33 (3), 397–411.

Munk, W.H., 1949. Surf beats. Trans. Am. Geophys. Union 30, 849–854.

Roelvink, J.A., Petit, H.A.H., Kostense, J.K., 1992. Verification of a one-dimensional surfbeat model against laboratory data. In: Proc. of the 23th Coastal Eng. Conf. ch. 72, pp. 960–973.

Roelvink, J.A., 1993. Surf beat and its effect on cross-shore profiles. Ph.D. thesis. Technical University of Delft.

Schäffer, H.A., 1990. Infragravity water waves induced by short-wave groups. Series paper No. 50. Ph.D. thesis. ISVA, Technical University Denmark.

Schäffer, H.A., Madsen, P.A., Deigaard, R., 1993. A Boussinesq model for waves breaking in shallow water. Coast. Eng. 20, 185–202.

Schäffer, H.A., 1993. Infragravity waves induced by short-wave groups. J. Fluid Mech. 247, 551–588.

Symonds, G., Huntley, G.A., Bowen, A.J., 1982. Two dimensional surf beat: Long wave generation by a time-varying break point. J. Geophys. Res. 87 (C1), 492–498.

Sørensen, O.R., Schäffer, H.A., Madsen, P.A., 1998. Surf zone dynamics simulated by a Boussinesq type model. Part III: Wave induced horizontal nearshore circulations. Coast. Eng.

Tucker, M.J., 1950. Surf beats: Sea waves of 1 to 5 min period. Proc. R. Soc. London Ser. A 202, 565–573.

Watson, G., Peregrine, D.H., 1992. Low frequency waves in the surf zone. In: Proc. of the 23th Coastal Eng. Conf. ch. 61, pp. 818–831.

Watson, G., Barnes, T.C.D., Peregrine, D.H., 1994. The generation of low frequency waves by a single wave group incident on a beach. In: Proc. of the 24th Coastal Eng. Conf. ch. 57, pp. 776–790.